

PROCEEDINGS OF SPIE

SPIDigitalLibrary.org/conference-proceedings-of-spie

Novel measurement of LV twist using 4DCT: quantifying accuracy as a function of image noise

Gabrielle M. Colvert, Ashish Manohar, Brendan Colvert, Andrew Schluchter, Francisco Contijoch, et al.

Gabrielle M. Colvert, Ashish Manohar, Brendan Colvert, Andrew Schluchter, Francisco Contijoch, Elliot McVeigh, "Novel measurement of LV twist using 4DCT: quantifying accuracy as a function of image noise," Proc. SPIE 10953, Medical Imaging 2019: Biomedical Applications in Molecular, Structural, and Functional Imaging, 109531K (15 March 2019); doi: 10.1117/12.2512532

SPIE.

Event: SPIE Medical Imaging, 2019, San Diego, California, United States

Novel measurement of LV twist using 4DCT: quantifying accuracy as a function of image noise

Gabrielle M. Colvert^a, Ashish Manohar^b, Brendan Colvert^a, Andrew Schluchter^a,
Francisco Contijoch^{a,c}, Elliot McVeigh^{a,c,d}

^aDepartment of Bioengineering; ^bDepartment of Mechanical Engineering; ^cDepartment of Radiology; ^dDepartment of Cardiology; University of California San Diego, 9500 Gilman Dr, La Jolla, CA 92093

ABSTRACT

Large trials have demonstrated the prognostic value of quantifying left ventricular (LV) twist because of its crucial role in the coupling of systolic and diastolic cardiac function. Current methods for measuring LV twist evaluate rotation in a 2D plane, chosen prospectively, and the data is acquired over multiple heartbeats. In this paper, a new method for assessing 3D endocardial LV twist from single-heartbeat, ECG-gated, 4DCT volumes is proposed.

In this study, the ability of the novel LV twist algorithm to accurately measure rotation in a mathematical phantom with known deformation is evaluated. The mathematical phantom was then 3D-printed to determine the accuracy of the rotation measurement from CT images in the presence of varying levels of noise. Lastly, as a proof-of-concept, LV twist was measured in human hearts across the cardiac cycle to determine whether reasonable estimates of endocardial rotation could be obtained from 4DCT studies of standard clinical quality.

In both the mathematical and 3D-printed phantoms (for $\text{CNR} \geq 9.3$), the measured LV twist was highly correlated ($r^2 \geq 0.98$, $p < 0.001$) with the known ground truth rotation function. In the healthy controls, the mean endocardial LV twist was found to be $25.3^\circ \pm 6.5^\circ$ and occurred within 30-36% of the R-R interval. From these results, it is clear that 3D rotational information and LV twist can be obtained from ECG-gated 4DCT volumes. The accuracy of LV twist in clinical data requires validation via a gold standard, such as MRI-tagging.

Keywords: Cardiac function, 4DCT, LV twist, torsion, rotation, cardiac mechanics, 3D-printing, contrast-to-noise

1. INTRODUCTION

The ordered structure of myocardial fibers within the left ventricle (LV) plays a crucial role in cardiac mechanics and function. The endocardial fibers follow a left-handed helix around the circumferential fibers within the midwall while the epicardial fibers follow a right-handed helix¹. The orientation of the endocardial and epicardial fiber helices causes the apex and base of the LV to rotate in opposite directions during contraction and relaxation. This wringing motion allows for normal ejection fractions of 60-70% even though myofibers only shorten by 15-20%². It also leads to the distribution of transmural stress and the storage of potential energy during systole³. The energy is subsequently utilized for diastolic recoil leading to efficient ventricular filling^{1,3}.

LV twist is a metric used to quantify the torsional motion of the left ventricle and is defined as the difference in rotation from the apex to the base. It has been identified as a more sensitive parameter than traditional functional measures, like ejection fraction, due to its important role in the coupling of systolic and diastolic function. In addition, large trials have demonstrated the prognostic value of measuring twist in various patient populations. For example, LV twist has been used to identify patients receiving chemotherapy drugs who are at risk of developing heart failure, for predicting positive remodeling in patients who underwent cardiac resynchronization therapy, and as an early indicator for heart transplant rejection³⁻⁷.

The current methods for measuring LV twist include speckle-tracking echocardiography and MRI-tagging. 2D speckle-tracking evaluates rotation in a plane which is chosen prospectively. Therefore, in order to quantify LV twist, multiple heartbeats must be acquired and the measurement is subject to through-plane motion^{1,2}. This modality has experienced poor reproducibility in normal values reported due to poor image quality, lack of the appropriate acoustic window, and inconsistency in the apical and basal planes chosen because of operator-related variability⁶. While the use of 3D speckle-tracking is starting to be implemented to combat the issue of through-plane motion, this modality is still subject to variable image quality, relies on highly skilled technicians, and requires multiple, regular-rhythm heartbeats for accurate data acquisition⁸.

Although MRI-tagging provides high-quality and reproducible rotation quantification, individual 4D sequences measure rotation in a 2D plane chosen prospectively over multiple heartbeats. In addition, it is more expensive and cannot be used in all patients who have implanted devices^{1,2}. There have been several attempts to extend the tagging technique to 3D space, however, these exams require prolonged scan times accompanied by lengthy periods of breath-holding which can be difficult for patients⁹.

This paper presents a new method for quantifying endocardial rotation and LV twist from ECG-gated 4DCT volumes collected in a single heartbeat. 3D motion is measured by tracking features on the endocardial surface of the LV using a nonrigid registration algorithm. Rotation and LV twist are then derived from this motion field at each timeframe across the cardiac cycle. This study aims to evaluate the novel measurement algorithm's ability to accurately evaluate rotation in a mathematical phantom with known deformation. The mathematical phantom was then 3D-printed to assess if rotation could be accurately measured from CT images obtained with a clinical protocol. Lastly, the LV twist algorithm was used to see if endocardial rotation could be estimated across the cardiac cycle in human subjects with normal cardiac function using 4DCT.

2. METHODS

2.1 Measuring 3D + time rotation with 4DCT

In order to measure endocardial rotation across the cardiac cycle, the LV was segmented from 4DCT images using ITK Snap (ver. 3.6.2)¹⁰. A threshold was chosen to distinguish the contrast-enhanced blood pool from the surrounding myocardium. This resulted in a cast of the endocardial surface with fiducial markers due to the papillary muscles and trabeculae within the chamber. These features were preserved in a surface mesh and tracked across time and 3D space using the coherent point drift (CPD) registration method previously used to measure endocardial strain¹¹. This process is summarized in Figure 1. After solving for the displacement of each volume from the template frame using CPD, Maximum Likelihood Estimation (MLE) was used to fit an affine transformation to each slice across the volume at each timeframe. All calculations were performed using MATLAB (2017a, Mathworks, Natick, MA).

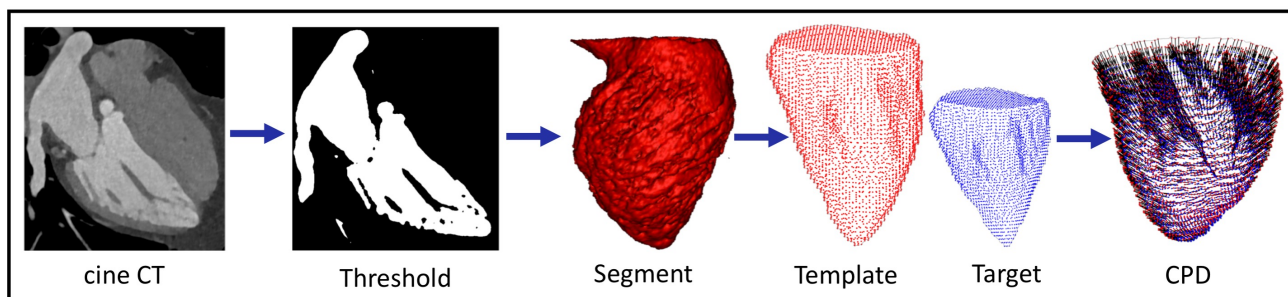


Figure 1: Pipeline for obtaining displacement field from CT images using non-rigid registration of endocardial surface meshes. N number of volumes within the cardiac cycle are thresholded to obtain only the LV blood pool and create a cast of the features on the endocardial surface. After segmentation, a surface mesh is created which preserves these features. A template mesh, usually end-diastole, is registered to the subsequent timeframes (target meshes) using the CPD algorithm. The result is a displacement field for the ventricle across the cardiac cycle and N total meshes with corresponding faces and vertices.

2.1.1 Determine affine transformation using Maximum Likelihood Estimation

After performing CPD registration, the point clouds were rotated from the axial position so that the z-axis was aligned with the long axis of the ventricle. Then, the template frame was divided into 2D slices based on the z-position of each vertex. Equivalent slices were found at subsequent timeframes using the CPD registered surface meshes containing point-to-point correspondence with the template mesh.

The set of reference points was denoted $\mathbf{X} \in \mathbb{R}^{2 \times n}$, where n is the number of vertices in the 2D slice. The reference timeframe was always chosen to be the end-diastolic phase. The motion of \mathbf{X} was modeled as the affine transformation

$$\mathbf{y} = \mathbf{A}\mathbf{X} + \mathbf{b} + \mathcal{R}, \quad (1)$$

where $\mathbf{A} \in \mathbb{R}^{2 \times 2}$ is the transformation matrix, $\mathbf{b} \in \mathbb{R}^2$ is the translation vector, $\mathcal{R} \in \mathbb{R}^2$ is the residual, and $\mathbf{y} \in \mathbb{R}^{2 \times n}$ is the result of the motion. The components of \mathbf{A} and \mathbf{b} were defined as

$$\mathbf{A} = \begin{bmatrix} a_{11} & a_{12} \\ a_{21} & a_{22} \end{bmatrix} \text{ and } \mathbf{b} = \begin{bmatrix} b_1 \\ b_2 \end{bmatrix}. \quad (2)$$

It was assumed that the residual is a normally distributed random variable with zero mean and isotropic variance

$$p_{\mathcal{R}}(\mathbf{r}) = \frac{1}{\sqrt{(2\pi)^2 |\Sigma|}} \exp\left(-\frac{1}{2} \mathbf{r}^T \Sigma^{-1} \mathbf{r}\right), \quad (3)$$

where Σ is the covariance matrix and defined as

$$\Sigma = \sigma \mathbf{I} = \begin{bmatrix} \sigma & 0 \\ 0 & \sigma \end{bmatrix}. \quad (4)$$

The random variable \mathbf{y} followed the same distribution function with a shifted mean $\boldsymbol{\mu} = \mathbf{A}\mathbf{x} + \mathbf{b}$, therefore

$$p_{\mathbf{y}}(\mathbf{y}) = \frac{1}{\sqrt{(2\pi)^2 |\Sigma|}} \exp\left(-\frac{1}{2} (\mathbf{y} - \mathbf{A}\mathbf{x} - \mathbf{b})^T \Sigma^{-1} (\mathbf{y} - \mathbf{A}\mathbf{x} - \mathbf{b})\right). \quad (5)$$

A parameter vector was defined as $\boldsymbol{\eta} = [a_{11} \ a_{12} \ a_{21} \ a_{22} \ b_1 \ b_2 \ \sigma]^T$. The likelihood function for a given data point $\{\mathbf{x}_n, \mathbf{y}_n\}$ is called $\mathcal{L}(\boldsymbol{\eta} | \{\mathbf{x}_n, \mathbf{y}_n\})$ and was found by evaluating the distribution at that data point

$$\mathcal{L}(\boldsymbol{\eta} | \{\mathbf{x}_n, \mathbf{y}_n\}) = p(\mathbf{x}_n, \mathbf{y}_n | \boldsymbol{\eta}). \quad (6)$$

The likelihood function for the entire 2D slice was given by

$$\mathcal{L} = \prod_n \mathcal{L}_n. \quad (7)$$

The negative log likelihood was then defined as

$$NLL = -\log(\mathcal{L}) = -\sum_n \log(\mathcal{L}_n). \quad (8)$$

In order to find the maximum likelihood estimate $\boldsymbol{\eta}^*$, NLL was minimized

$$\boldsymbol{\eta}^* = \underset{\boldsymbol{\eta}}{\operatorname{argmin}} NLL(\boldsymbol{\eta}). \quad (9)$$

The minimization of NLL in order to find the maximum likelihood estimate for $\boldsymbol{\eta}$ was performed using MATLAB's built in nonlinear solver *fmincon*. The initial conditions for each of the parameters were

$$\mathbf{A}_0 = \begin{bmatrix} 1 & 0 \\ 0 & 1 \end{bmatrix}, \mathbf{b}_0 = \begin{bmatrix} 0 \\ 0 \end{bmatrix}, \text{ and } \sigma_0 = 1000, \quad (10)$$

which assumed zero scaling, shear, rotation, and translation. Because of this, σ_0 was initialized to a large enough value to account for the variability in vertex position within the slice. Lastly, an additional constraint was added to ensure σ was non-negative.

2.1.2 Calculating rotation angle and determining uncertainty

Once $\boldsymbol{\eta}^*$ was calculated for each slice in z across the ventricle for each timeframe, the rotation matrix, \mathbf{R}^* , was found by using singular value decomposition of the matrix \mathbf{A}^* and defined as

$$\mathbf{R}^* = \begin{bmatrix} r_{11}^* & r_{12}^* \\ r_{21}^* & r_{22}^* \end{bmatrix} \quad (11)$$

The rotation angle, derived from the rotation matrix, was defined as

$$\theta^* = \tan^{-1} \left(\frac{r_{12}^*}{r_{11}^*} \right). \quad (12)$$

This coordinate definition was chosen to designate counterclockwise rotation as a positive angle. This corresponds with the clinical convention that the counterclockwise rotation of the apex (as viewed from the apex toward the base) is a positive angle while the clockwise rotation of the base is negative¹².

The uncertainty in degrees on the estimated θ^* was estimated by

$$\delta = \tan^{-1} \left(\frac{\sigma^*}{\tilde{r}} \right), \quad (13)$$

where σ^* is the variance determined by the MLE of the affine transformation and \tilde{r} is the median radius of the slice.

2.2 Mathematical phantom

The ability for CPD to accurately capture the torsional displacement of the ventricle was tested using a mathematical phantom with known physiologic deformations. The *in-silico* phantom was created from the end-diastolic phase of a clinical scan of a healthy heart with normal cardiac function. The LV blood pool was first segmented using ITK snap. Then, the segmentation was made to have an isotropic resolution of 0.5 mm prior to rotation into alignment with long axis. Lastly, the endocardial surface mesh was extracted using MATLAB's *isosurface* tool. Displacements were then applied to the end-diastolic points based on literature-derived values of longitudinal and circumferential strain and torsion¹³⁻¹⁵ (Figure 2a). These deformations resulted in an ejection fraction of 71% as measured by CT volume¹⁶. For each set of x-y points at a uniform z-position, a rotation about the long axis from the center of mass of the slice was defined and is shown in Figure 2b. The rotation angle at the apex of the endocardial chamber was 13° which linearly decreased to -6.9° at the mitral valve plane giving a total twist of 19.9° from apex to base of the ventricle. (Positive angles are measured as counter-clockwise rotations when viewed from apex to base.)

CPD was used to solve for the displacement field between the template end-diastolic phase and the target end-systolic phase in order to evaluate the variation in rotation measurement due to registration errors alone. In clinical cases, because the volume of the end-systolic ventricle is smaller than at end-diastole, the mesh generated typically has 50% fewer vertices. Therefore, in order to simulate a clinical scan and disrupt the exact point-to-point coherence between

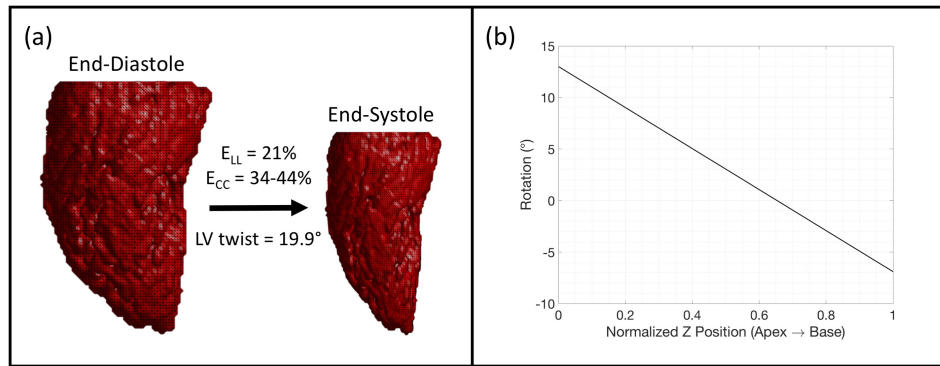


Figure 2: Known displacements applied to the mathematical phantom. a) Longitudinal and circumferential strain and LV twist were applied to the end-diastolic endocardial surface mesh to achieve a physiologic end-systolic phase for the analytical phantom. b) A rotation angle defined from the center of the ventricle was assigned to each set of x-y points as a linear function of z from tip of the endocardial chamber ($z = 0$) to the mitral valve plane ($z = 1$).

phases, noise was incorporated into the end-systolic mesh and 50 percent of the vertices were removed before running CPD. Then, rotation as a function of z-position was calculated using the CPD-registered meshes and compared to the known ground truth. This mathematical phantom was also used to find the optimal set of parameters for the registration algorithm as discussed by Manohar *et al.*¹⁷.

2.3 3D-printed phantom

The end-diastolic and end-systolic phases of the mathematical phantom were 3D-printed to see if rotation could be accurately measured from CT images in the presence of image noise. The phantoms were printed using a Form 2 stereolithography system with a clear photopolymer resin (Formlabs Inc., Somerville, MA). The segmentation of the blood pool and subsequent extraction of the mesh with features required for accurate CPD registration is dependent on the contrast between the LV and the myocardium. Therefore, both phases were scanned with decreasing mA levels and a tissue equivalent “extension ring” (Extension-Ring-Tissue (L, H200), QRM GmbH, Moehrendorf, Germany) to reduce the contrast-to-noise (CNR) ratio between these two regions.

All images were obtained on a Revolution CT scanner (GE Healthcare, Chicago, IL) using a small focal spot, standard reconstruction kernel, ASIR-V at 50% level, pixel spacing of 0.39 mm x 0.39 mm x 0.625 mm, and 100 kVp. The chamber was filled with x-ray contrast agent (Visipaque (iodixanol) 320mg Iodine/mL) diluted to 10% in water to mimic typical LV enhancement seen in clinical scans. The two phases of the 3D-printed phantom were first scanned at 450 mA with no extension ring to obtain the highest CNR image. This represented an optimal imaging scenario with minimal amount of noise. Then, this scan was repeated with the extension ring to simulate the attenuation of the human body. Inside the extension ring, the two phantoms were also scanned at 225 mA, 110 mA, and 50 mA to increase the image noise level.

To extract the endocardial surface meshes from the CT images, the method summarized in Figure 1 was used. All the images were down-sampled to an isotropic resolution of 1.25 mm prior to mesh extraction due to data size and registration time constraints. CPD was then used to find the displacement field from end-diastole to end-systole under each of the five scanning conditions. The rotation as a function of z-position was calculated using the CPD output and compared to the ground truth. Correlation plots were created to evaluate the accuracy of CPD-based angle measurements compared to the ground truth rotation angles.

2.4 Clinical data: healthy controls

To demonstrate the possibility of estimating LV twist from clinical ECG-gated 4DCT scans, 6 subjects who had normal LV function were evaluated. They had an ejection fraction of $68.9\% \pm 4.4\%$ and no observable motion or functional abnormalities. Each subject had a single-heartbeat, retrospective cardiac 4DCT data set with images at least every 10% of the cardiac cycle with slice thickness of 0.5 mm or 0.625 mm. The endocardial surface meshes for each timeframe were

obtained using the method described in Figure 1. As with the phantom data, the segmented volumes were downsampled to 1.25 mm (0.625 mm slice thickness) or 1.5 mm (0.5 mm slice thickness) isotropic resolution for computational considerations before mesh extraction. All timeframes were registered using CPD with the end-diastolic phase as the template mesh.

Rotation from end-diastole to all other phases within the cardiac cycle was calculated from the apex of the endocardial chamber to the mitral valve plane. From the results of the phantom data, it was clear that the accuracy of the rotation estimate decreases at both ends of the ventricle. Therefore, the most-apical slice was defined as 10% of the total LV length along the central long axis direction, and the most-basal slice was defined as 90% of the LV length. A linear fit of the rotation angle vs position along the LV length was used to calculate LV twist. A low-pass filter was applied to the time-based curves of LV twist to smooth noisy estimates due to motion artifacts in certain phases.

3. RESULTS

3.1 Mathematical Phantom

To demonstrate the variation in the measurement of rotation across the ventricle due to registration errors alone, CPD was used on the mathematical phantom to solve for the motion between the end-diastolic and end systolic phases. As shown in Figure 3a, there was a larger uncertainty in the rotation angle estimate towards the apex of the endocardial chamber ($z = 0$) due to the smaller radius and low number of points in those slices. This result showed that small errors occur at the apex without additional errors introduced by the imaging and post-processing procedures. This limitation led to the definition of the apex as 10% of the LV in order to avoid a region where errors are likely to affect the LV twist measurement more significantly. Overall, the measured rotation angles were highly correlated with the known ground truth rotation function applied to the mathematical phantom with $r^2 \cong 1$ and $p < 0.001$ (Figure 3b).

The mathematical phantom was also used to find the optimal set of parameters for CPD's non-rigid (lowrank) registration process which yielded the most accurate rotation measurement. The parameters that were chosen based on the optimization process and used for all the phantom and clinical data are listed in Table 1. Manohar *et al.* used an outlier weight of 0.05 because the mathematical phantom only had white noise, not true outliers¹⁷. In this study, the parameter was increased to 0.1 to account for outliers in seen in clinical images.

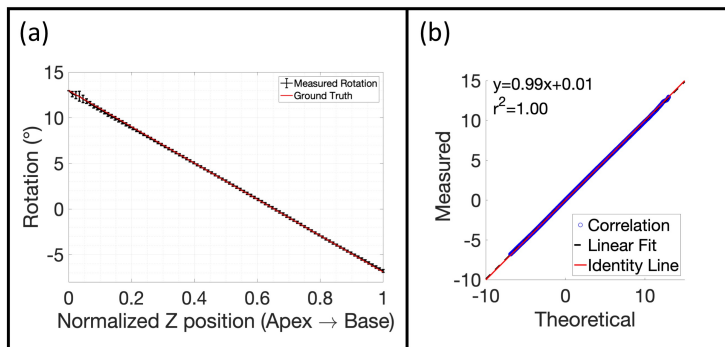


Figure 3: Accuracy of LV twist in the mathematical phantom. a) MLE rotation estimate per slice in z from the tip of the endocardial chamber to the mitral valve plane. The ground truth rotation function is shown in red. b) Correlation plot for measured vs. theoretical ground truth rotation angles.

Parameter	Value
β	1.1
λ	11
outliers	0.1
numeig	100

Table 1: Parameters for the nonrigid (lowrank) CPD registration algorithm chosen from the optimization process described by Manohar *et al.* which gave the best estimate of rotation.

3.2 3D-printed Phantom

The mathematical phantom was 3D-printed to examine the accuracy of rotation estimates from CT images with increasing image noise. From the 5 imaging scenarios, the CNR was calculated with the regions in Figure 4a for the LV and myocardium using the equation in Figure 4b. As shown in Figure 4c, the highest CNR images were those with the

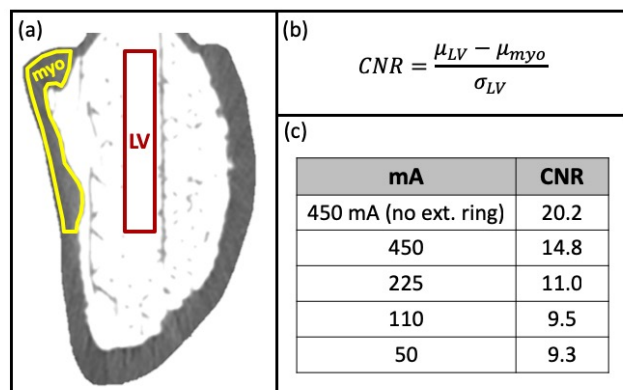


Figure 4: Calculation of CNR in 3D-printed phantom. a) Sample LV and myocardium regions used to calculate CNR. b) Equation used to calculate CNR where μ is the mean intensity within the region and σ is the standard deviation. c) Tube current resulting CNR for the 5 imaging scenarios. The extension ring was used in all cases except the first one.

highest tube current (450 mA) and no extension ring. As the mA decreased and the extension ring was included, the image noise increased and CNR was reduced. The reduction in CNR was less drastic than expected at 50 mA with the extension ring, however, this was likely due to the ASIR-V level which was set at 50% to match the reconstruction settings of clinical scans.

While the decrease in CNR affected the accuracy of the LV twist measurement, the correlation in all cases was still very good ($r^2 \geq 0.98$ and $p < 0.001$) for $CNR \geq 9.3$ (Figure 5). However, there was higher uncertainty and disagreement with the ground truth angles near the apex as seen in the mathematical phantom. There was also a higher disagreement between the measured and ground truth rotation towards the middle of the ventricle. This was most likely due to the location of the papillary muscles which made the registration more difficult. Towards the base, the cap on the surface mesh also added uncertainty in the final few slices. Therefore,

the most-basal segment used to measure LV twist in the clinical data was defined as 90% of the LV.

3.3 Clinical data: Twist measured in the normal LV

As a proof-of-concept to see if the torsional motion of the endocardium could be captured in ECG-gated clinical CT scans, CPD-derived LV twist was measured in healthy subjects. At every timeframe within the cardiac cycle, rotation of each slice from the apex of the endocardial chamber to the mitral valve plane was calculated. A linear fit of these rotation estimates from the apex (10% of the LV) to the base (90% of the LV) was used to calculate LV twist. Figure 6 shows the linear fit for each of the 6 subjects at the timeframe where the maximum slope occurred. The maximum LV twist in the

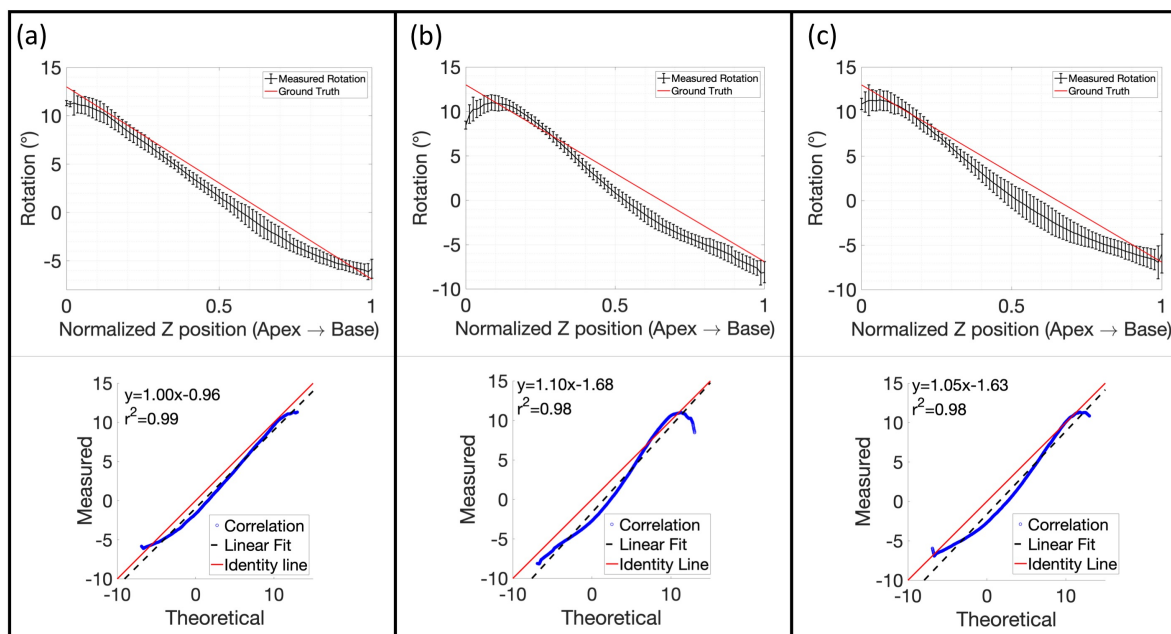


Figure 5: Accuracy of 3D-printed phantom vs image noise. MLE rotation estimate for each slice in z compared to ground truth rotation function (top) and correlation plots (bottom) for a) $CNR=20.2$, 450 mA, no extension ring, b) $CNR=14.8$, 450 mA with extension ring, and c) $CNR=9.3$, 50 mA with extension ring.

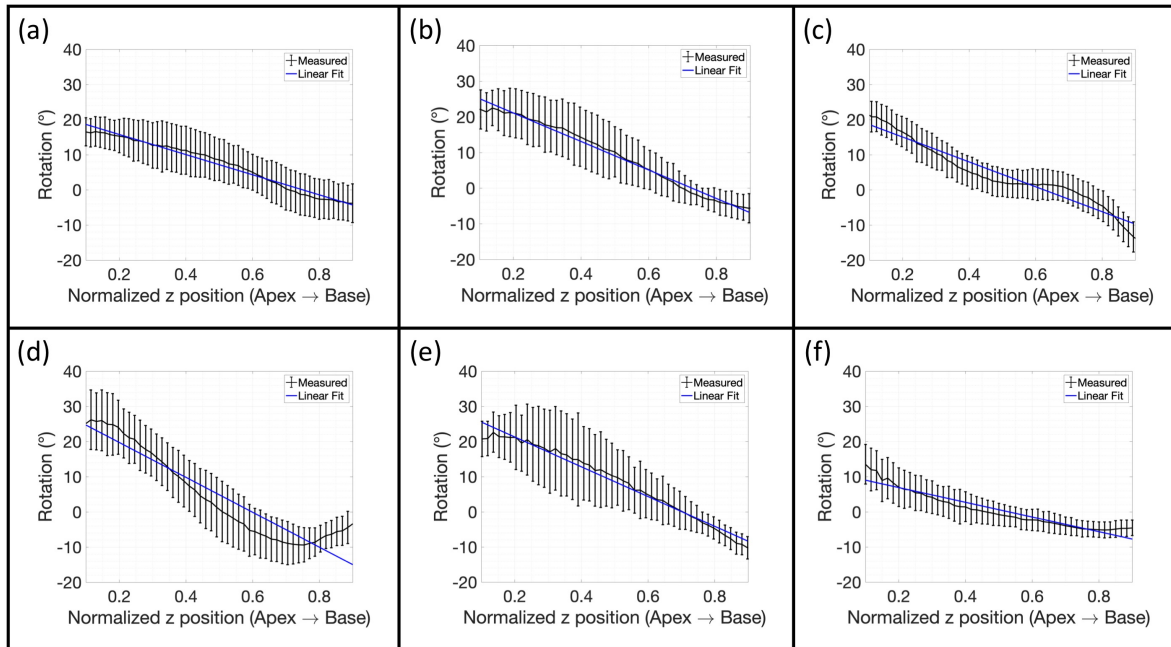


Figure 6: Linear fit of rotation estimates for subjects with normal LV function. (a-e) For each of the 6 subjects the linear fit from apex ($z=0.1$) to base ($z=0.9$) is shown in blue for the timeframe with the maximum slope, or maximum LV twist. In black is the measured rotation angle per long axis slice with the uncertainty which is estimated from σ^* of the MLE fit as described in equation 13.

normal subjects was $25.3^\circ \pm 6.5^\circ$ and within 30% to 36% of the R-R interval (Figure 7). The mean apical rotation at maximum LV twist was $20.2^\circ \pm 6.3^\circ$ and the mean basal rotation was $-8.6^\circ \pm 3.6^\circ$.

4. DISCUSSION

4.1 Main findings

Routine clinical methods for measuring LV twist, such as speckle-tracking echocardiography and MRI-tagging, assess rotation in 2D planes subject to through-plane motion and the data must be acquired across multiple heartbeats. This manuscript proposes a novel method for quantifying 3D endocardial LV twist from single-heartbeat ECG-gated 4DCT scans. The rotation, and subsequently LV twist, was derived from displacement fields obtained from tracking the features on the endocardial surface using CPD, a nonrigid registration algorithm. The accuracy of this method was evaluated in both a mathematical and 3D-printed phantom. In both cases, the measured rotation values were highly correlated with the theoretical rotation values.

Once it was determined that endocardial rotation could be measured with CT images, LV twist was computed in 6 subjects who had normal LV function. From these results, it was clear that a LV twist signal could be obtained across the cardiac cycle as demonstrated in Figure 7. The maximum LV twist of $25.3^\circ \pm 6.5^\circ$ was higher than reported values in normal subjects of $20.0^\circ \pm 7.3^\circ$ ¹⁴. This could be due to the fact that the proposed method measures endocardial motion which is known to have higher strain values¹⁸. In addition, the higher

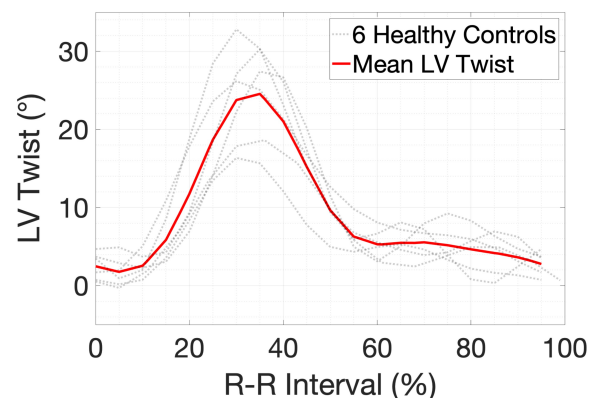


Figure 7: LV twist vs. time in subject with normal LV function. For all 6 subjects LV twist with respect to the end-diastolic frame is shown across the cardiac cycle. The mean LV twist is displayed in red.

LV twist value was derived from 3D data as compared to the reported values from 2D clinical methods. However, because a ground truth was lacking for these patients, the next step is to validate the proposed method against MRI-tagging in patients who receive a clinical CTA and CMR study in the same day.

4.2 Limitations

As demonstrated in the phantom experiments, the measurement of LV twist is highly dependent on the accuracy of CPD. Although the mathematical phantom was used to find the optimal parameters for the registration algorithm, there were still errors in the measurement because the fit was not perfect. The addition of image noise and motion artifacts affects the registration process, however, these factors were not fully simulated in the mathematical phantom. In addition, the lowest CNR observed was 9.3 with 50 mA. Therefore, a significant decline in the measured twist values was not observed. Future studies will decrease the concentration of iodine in the chamber to decrease the CNR further and observe at what CNR the measurement fails.

Mid-systolic frames can have motion artifacts which limit the accuracy of the rotation estimates. In this study, a lowpass filter was used on the time curves to smooth these noisy estimates. Motion artifacts could also be addressed by improved reconstruction techniques, such as SnapShot Freeze (GE Healthcare)¹⁹.

Although CT provides a high resolution map of the endocardial surface which can be used to quantify LV function, there are radiation dose concerns associated 4DCT. In this study, multiple phases across the R-R interval were used in order to assess maximal twist and calculate multiple independent estimates of LV twist vs. time. However, in clinical practice, only two phases are needed to calculate the twist value for a patient.

5. CONCLUSION

This was the first time that 3D + time rotation was measured from single heartbeat 4DCT images using feature tracking of the endocardial surface. It was demonstrated that CPD, a nonrigid registration algorithm, is capable of accurately measuring LV twist. In addition, CT images can be used to quantify ventricular torsion in a 3D-printed phantom with known deformations. Lastly, rotational information can be assessed in patients from ECG-gated 4DCT volumes which are clinically obtained to measure ventricular function or coronary anatomy. The accuracy of the LV twist algorithm requires validation against a gold-standard method such as MRI-tagging.

ACKNOWLEDGEMENTS

This work was supported by a grant from the National Institutes of Health, USA (NIH grant T32 HL 105373)

We thank Dr. Marcus Chen at the Laboratory of Cardiac Energetics, NHLBI, for providing human CT data used in this work.

REFERENCES

- [1] Sengupta, Partho P., Tajik A. Jamil, Chandrasekaran, K. and Khandheria, B. K., "Twist Mechanics of the Left Ventricle," *JACC Cardiovasc. Imaging* **1**(3), 366–376 (2008).
- [2] Nakatani, S., "Left Ventricular Rotation and Twist: Why Should We Learn?," *J. Cardiovasc. Ultrasound* **19**(1), 1 (2011).
- [3] Stöhr, E. J., Shave, R. E., Baggish, A. L. and Weiner, R. B., "Left ventricular twist mechanics in the context of normal physiology and cardiovascular disease: a review of studies using speckle tracking echocardiography," *Am. J. Physiol. - Hear. Circ. Physiol.* **311**(3), H633–H644 (2016).
- [4] Mornoş, C. and Petrescu, L., "Early detection of anthracycline-mediated cardiotoxicity: the value of considering both global longitudinal left ventricular strain and twist¹," *Can. J. Physiol. Pharmacol.* **91**(8), 601–607 (2013).
- [5] Bertini, M., Sengupta, P. P., Nucifora, G., Delgado, V., Ng, A. C. T., Marsan, N. A., Shanks, M., van Bommel, R. R. J., Schalij, M. J., Narula, J. and Bax, J. J., "Role of Left Ventricular Twist Mechanics in the Assessment of Cardiac Dyssynchrony in Heart Failure," *JACC Cardiovasc. Imaging* **2**(12), 1425–1435 (2009).

- [6] Thavendiranathan, P., Poulin, F., Lim, K. D., Plana, J. C., Woo, A. and Marwick, T. H., "Use of myocardial strain imaging by echocardiography for the early detection of cardiotoxicity in patients during and after cancer chemotherapy: A systematic review," *J. Am. Coll. Cardiol.* **63**(25 PART A), 2751–2768 (2014).
- [7] Omar, A. M. S., Vallabhajosyula, S. and Sengupta, P. P., "Left Ventricular Twist and Torsion Research: Observations and Clinical Applications," *Circ Cardiovasc Imaging* **8**(6), 74–82 (2015).
- [8] Muraru, D., Niero, A., Rodriguez-Zanella, H., Cherata, D. and Badano, L., "Three-dimensional speckle-tracking echocardiography: benefits and limitations of integrating myocardial mechanics with three-dimensional imaging," *Cardiovasc. Diagn. Ther.* **8**(1), 101–117 (2018).
- [9] Ibrahim, E. S. H., "Myocardial tagging by cardiovascular magnetic resonance: evolution of techniques--pulse sequences, analysis algorithms, and applications.," *J. Cardiovasc. Magn. Reson.* **13**(1), 36 (2011).
- [10] Yushkevich, P. A., Piven, J., Hazlett, H. C., Smith, R. G., Ho, S., Gee, J. C. and Gerig, G., "User-guided 3D active contour segmentation of anatomical structures: Significantly improved efficiency and reliability," *Neuroimage* **31**(3), 1116–1128 (2006).
- [11] Pourmorteza, A., Schuleri, K. H., Herzka, D. A., Lardo, A. C. and McVeigh, E. R., "A New Method for Cardiac Computed Tomography Regional Function Assessment: SQUEEZ," *Circ Cardiovasc Imaging* **5**, 243–250 (2012).
- [12] Tavakoli, V. and Sahba, N., "Assessment of age-related changes in left ventricular twist by 3-dimensional speckle-tracking echocardiography.," *J. Ultrasound Med.* **32**(8), 1435–1441 (2013).
- [13] Shi, J., Pan, C., Kong, D., Cheng, L. and Shu, X., "Left Ventricular Longitudinal and Circumferential Layer-Specific Myocardial Strains and Their Determinants in Healthy Subjects," *Echocardiography* **33**(4), 510–518 (2016).
- [14] Kocabay, G., Muraru, D., Peluso, D., Cucchini, U., Mihaila, S., Padayattil-Jose, S., Gentian, D., Iliceto, S., Vinereanu, D. and Badano, L. P., "Normal left ventricular mechanics by two-dimensional speckle-tracking echocardiography. Reference values in healthy adults. [Spanish]rMecanica ventricular izquierda normal mediante ecocardiografi a speckle tracking bidimensional. Valores de referencia pa," *Rev. Esp. Cardiol.* **67**(8), 651–658 (2014).
- [15] Moore, C. C., McVeigh, E. R. and Zerhouni, E. A., "Quantitative tagged magnetic resonance imaging of the normal human left ventricle," *Top. Magn. Reson. Imaging* **11**(6), 359–371 (2000).
- [16] McVeigh, E. R., Pourmorteza, A., Guttman, M., Sandfort, V., Contijoch, F., Budhiraja, S., Chen, Z., Bluemke, D. A. and Chen, M. Y., "Regional myocardial strain measurements from 4DCT in patients with normal LV function," *J. Cardiovasc. Comput. Tomogr.* (2018).
- [17] Manohar, A., Colvert, G., Schluchter, A., Contijoch, F. and Elliot, R., "LV Systolic Point-Cloud Model to Quantify Accuracy of CT Derived Regional Strain (SQUEEZ)," *SPIE Med. Imaging Conf. Proc.* (2019).
- [18] Sorger, J., Wyman, B. T., Faris, O. P., Hunter, W. C. and McVeigh, E. R., "Torsion of the Left Ventricle During Pacing with MRI Tagging," *J Cardiovasc Magn Reson.* **5**(4), 521–530 (2003).
- [19] Nett, B. E., Pack, J. D. and Okerlund, D., "Task based assessment of a motion compensation algorithm via simulation of a moving stenotic vessel," *Proc. SPIE*(March 2013), 86682B (2013).